

# STRESS CONTOURS IN THE CONNECTING-ROD UNDER THE DYNAMIC LOAD AND THE OIL FILM'S PRESSURE OF THE CONNECTING-ROD BIG END

**Tran Thi Thanh Hai**

*Hanoi University of Science and Technology, 1 Dai Co Viet Road, Ha Noi, Viet Nam*

\*Email: [hai.tranthithanh@hust.edu.vn](mailto:hai.tranthithanh@hust.edu.vn)

Received: 16 September 2019; Accepted for publication: 6 January 2020

**Abstract.** Load applied to the connecting-rod and the pressure in the lubricant oil film change the stress in the connecting-rod during the operating cycle. This problem is one of the characteristics we need to consider when studying the connecting-rod big end bearing. A specific experimental device and the connecting-rod model of photoelastic material are used to determine the load diagram, measure the oil film pressure, and visualize the state of stress. The connecting-rod is subjected to simulation load as in the engine. The lubricated oil film pressure is measured by the pressure sensor and also calculated by numerical modelization method with the same load diagram. The method chosen to visualize the stress state in the dynamically loaded connecting rod is the transmission photoelasticimetry. This method allows the visualization of the isochrones fringes, which are lines of equal difference regarding main stresses in the connecting-rod. The stress contour's images of the connecting-rod at different angles of the crankshaft are realized by a CCD camera. The measured stress contours are compared to the calculated stress contours by the Algor software. The results show globally a correspondence between the experimental isochrones fields and the calculated isochrones fields.

*Keywords:* lubrication, connecting-rod, bearing, pressure, stress.

*Classification numbers:* 5.4.3, 5.4.4, 5.10.1.

## 1. INTRODUCTION

The elastohydrodynamic lubrication (EHD) of the connecting-rod big end bearing is a complex problem because several parameters have influence on the behaviour of the oil film and on the solids. For a few decades, the elastohydrodynamic lubrication problems have been commonly studied. Fantino *et al.* [1] proposed a solution for EHD problem for a short bearing subjected to dynamic loads. Oh and Goenka [2] studied the extent of the active and inactive zones in the film of the transient EHD of a connecting-rod big end bearing. The problem of free borders is formulated like a complementary problem and dealt by Murty's algorithm. In 2001, Bonneau and Hajjam [3] presented a new algorithm based on JFO's model. This algorithm ensures to monitor the rupture and reformation of the lubricating film in the contact EHD. In 2004, Wang *et al.* [4] presented a study which takes into account the deformations due to the tightening of the screw during the functional cycle. They considered also the influence of the

---

inertia effects and the total deformation of the connecting-rod on the lubricated parameters. In 2006, Tran T.T. Hai [5] studied the numerical modeling of the behavior of the connecting rod big end bearings requiring to account for the interdependence of the effects of the interfaces fluid, between connecting rod and the journal, and solid in the mating surface between the body and the cap.

Parallel to these numerical modeling, many experimental studies are carried out to determine the connecting-rod big end bearing behaviour. Bates *et al.* [6] measured the oil film thickness by the capacitive method. In 2000, Optasanu [7] used the method of analysis per correlation of digital images and photoelasticity to measure respectively the film thickness and to visualize the state of stresses generated in the connecting-rod. He measured the film thickness, the pressure and the temperature of lubricating film versus the mode of the crankshaft. Fatu [8] in 2005 developed a test bench to study the lubrication of the connecting-rod big end bearings under real and severe operating conditions. The maximum engine speed can reach 20000 rpm with loads applied of 90 kN in compression and 60 kN in traction. In 2019, Tran T T Hai *et al.* [9] studied the influence of the radial clearance on the pressure distribution of the 5S-FE engine's connecting-rod big end bearing. The radials of the connecting-rod are measured at different screw tightening.

This study presents the experimental stress state of the connecting-rod model and the calculated stress contours by the Algor software.

## 2. EXPERIMENTAL STRESS STATE OF THE CONNECTING-ROD

### 2.1. Experimental device

The experimental device (Figure 1) respects the kinematics of connecting-rod crank system and the connecting-rod model. The connecting-rod model is formed by a rigid small end (8) and a big end in photoelastic material (9a and 9b) [10,11].

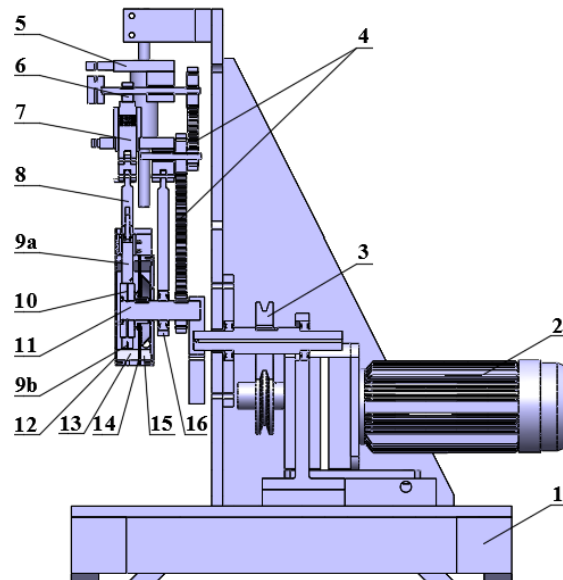


Figure 1. Functional scheme of the experimental device.

It is placed parallel with master connecting-rod. The studied connecting-rod big end formed by a body (9a), a cap (9b) and the journal (10) form a smooth bearing. An electric motor (2) rotates the crankshaft (11) by the reduction gear. The rotation speed of the crankshaft is ranged between 0 and 250 rpm. A master steel connecting-rod (16) is linked to the journal and it is fixed to master piston (5). This system can slide on two solid parallel pillar of the main body (1). During the operation, the master connecting-rod alternatively pushes the piston to the top and pulls it to the underneath. This resulting motion has the classic movement of connecting-rod crank system in the internal combustion engine. The piston (8) plays the role of piston in a real combustion engine. To simulate the explosion as in a real engine, which occurs a turn on two in a 4 - stroke engine, the axis of the camshaft (6) turns twice more slowly than the crankshaft (11). The action of the camshaft on the push rod compress the spring which in turn exerts a force on the small end that thus simulates the explosion in an engine. The study in connecting-rod is immersed in an oil chamber.

The Figure 2 is the photograph of the experimental device with the measurement system.

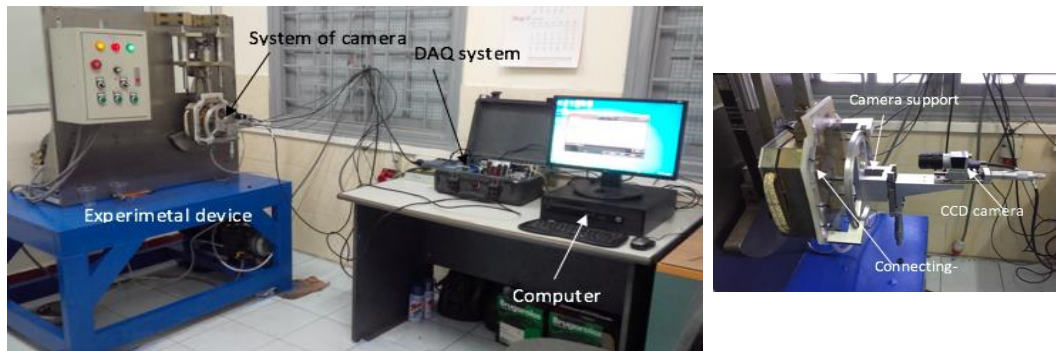


Figure 2. Photograph of the experimental device.

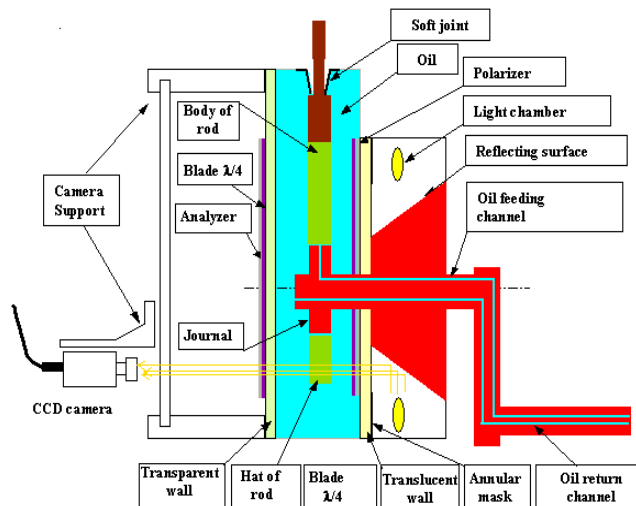


Figure 3. Lighting system, oil feeding channel.

Figure 3 presents the light system and the oil feeding channel. The light system is placed in a room behind the oil chamber. This light source, the  $\frac{1}{4}$  wave blades, the polarizer and analyzer constitute a circular polariscope to visualize the isochromatic. The oil feeding system for

studying bearing consists of an oil tank, a hydraulic pump, a manometer, a rotating distributor and two distribution channels which cross all along the length of the crankshaft. One of the channels is used to feed oil for the bearing. A CCD camera support follows the same movement that the connecting-rod and thus makes it possible to photograph in detail the connecting-rod during the functional cycle. Tables 1, 2 and 3 present the geometric characteristics of the big-end bearing, the characteristics of the lubricating oil, as well as the operating conditions of the device.

Table 1. Parameters of connecting-rod big end bearing.

Rotational Frequency	0 to 250	rpm
Bearing diameter	97	mm
Bearing radial clearance	0,3	mm
Connecting-rod thickness	20	mm
Length of the connecting-rod	257	mm

Table 2. Characteristics of the connecting-rod.

Density	$\rho_c$	1200	$\text{Kg/m}^3$
Young modulus	$E_c$	3150	MPa
Coefficient of thermal expansion	$\alpha_c$	$22.10^{-6}$	1/K
Thermal conductivity	$k_c$	0.18828	W/m.K
Poisson coefficient	$\nu_c$	0.36	
Photoelastic constant of PLM-4R		0.32	kPa/fringe/m

Table 3. Characteristics of silicone oil.

Density	$\rho_s$	980	$\text{Kg/m}^3$
Viscosity at 40 °C	$\mu_0$	0.33	Pa.s

## 2.2. Visualization method of stress state methods

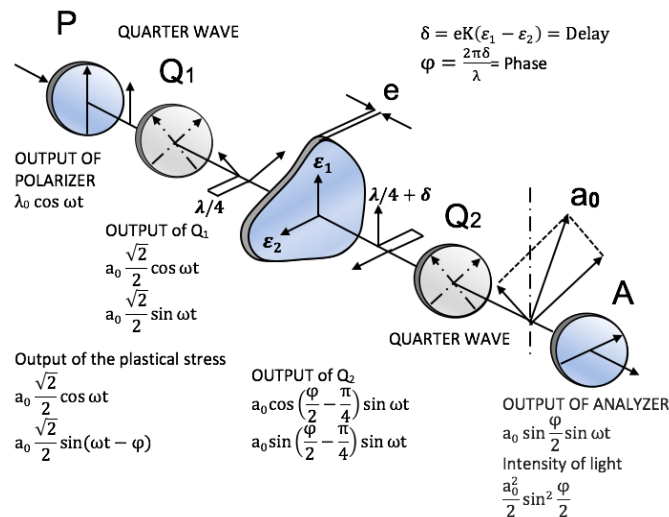


Figure 4. The optical assembly scheme used for visualization isochrones fields.

---

The optical assembly that allows to visualize the isochrones fields that is used in the study [12]. The method chosen to visualize the stress state in the dynamically loaded connecting rod is the transmission photoelasticimetry. This method allows the visualization of the isochrones fringes, which are lines of equal difference regarding main stresses in the connecting rod. Figure 4 shows the optical assembly scheme used for the visualization of the isochrones fringes. It consists of a polarizer, two quarter wave blades and an analyzer.

### 2.3. Experimental visualization of isochrones field

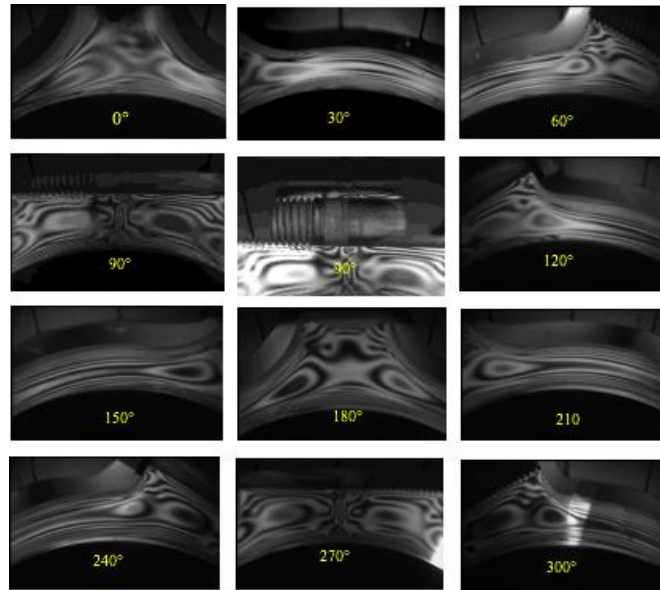


Figure 5. Isochrones field's images of the connecting-rod at a 360° crankshaft angle, rotation speed of 150 rpm.



Figure 6. Isochrones field of the connecting-rod big end bearing.

Using the image acquisition and processing software can photograph images. The isochrones field on the whole of the connecting-rod is obtained by the embarked CCD camera which allows a precise positioning of the camera. Figure 5 presents a series of images of isochrones fields from different areas of the connecting rod at a crank angle of 360° and a rotational speed of 150 rpm. The images of the different areas are repositioned using Adobe Photoshop software to obtain the total isochrones field of the big-end bearing (Figure 6).

### 3. MODELLING STRESS STATE OF THE CONNECTING-ROD

#### 3.1. Equation of the problem

##### The modified Reynolds equation

The hypothesis of an incompressible fluid, the Reynolds equation is written [13,14]:

$$\frac{\partial}{\partial x} \left( \frac{h^3}{6\mu} \frac{\partial p}{\partial x} \right) + \frac{\partial}{\partial z} \left( \frac{h^3}{6\mu} \frac{\partial p}{\partial z} \right) = U \frac{\partial h}{\partial x} + 2 \frac{\partial h}{\partial t} \quad (1)$$

For inactive zones (zone in cavitation), the Reynolds equation is reduced to (2) since the pressure which prevails there is constant (equal to the saturation vapor pressure  $p_{cav}$  or to the ambient pressure according to whether there is cavitation or separation).

$$U \frac{\partial \rho h}{\partial x} + 2 \frac{\partial \rho h}{\partial t} = 0 \quad (2)$$

where,  $\rho$  is the density of the lubricant-gas mixture due to the rupture of the lubricated film. Defining the filling  $r$ :

$$r = \frac{\rho h}{\rho_0}$$

with  $\rho_0$  is the density of the lubricant, the equation (2) is written:

$$U \frac{\partial r}{\partial x} + 2 \frac{\partial r}{\partial t} = 0 \quad (3)$$

The equations (1) and (3) are grouped into one using a universal variable  $D$  and the modified Reynolds equation to the form:

$$F \frac{\partial}{\partial x} \left( \frac{h^3}{6\mu} \frac{\partial D}{\partial x} \right) + F \frac{\partial}{\partial z} \left( \frac{h^3}{6\mu} \frac{\partial D}{\partial z} \right) = U \frac{\partial h}{\partial x} + 2 \frac{\partial h}{\partial t} + (1 - F) \left( U \frac{\partial D}{\partial x} + 2 \frac{\partial D}{\partial t} \right) \quad (4)$$

- for the active zones: 
$$\begin{cases} D = p & ; & D \geq 0 \\ F = 1 \end{cases}$$

- for the cavitation zones: 
$$\begin{cases} D = r - h & ; & D < 0 \quad (\rho < \rho_0) \\ F = 0 \end{cases}$$

The boundary conditions used to solve the Reynolds equation are based on the separation of the active and inactive zones. In the active zone, the pressure is established and equilibrated with the applied load. In the inactive zone, the pressure is lower than the atmospheric pressure. Figure 7 presents the proposed field of study. It comprises an inactive zone  $\Omega_0$  and an active zone  $\Omega$  separated by a boundary. For the same ordinate  $z$ , there will be, for example, a film rupture point located at  $x_r$  and another film reforming located at  $x$ .

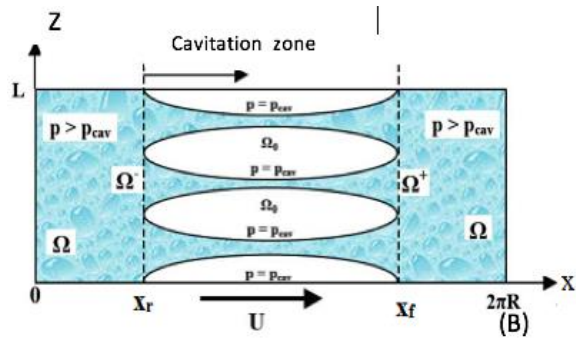


Figure 7. The active zone and inactive zone in the developed domain.

- On the external borders  $z = 0$  and  $z = L$   
 $p = p_o ; D = p_o ; p_o$  is the ambient pressure
- On the borders  $x = 0$  and  $x = B$   
 $D_{x=0} = D_{x=B}$  continuity of the D function
- On the border rupture or cavitation  $\Omega^-$   
 $p = p_{cav} ;$  In the zone  $\Omega_0 : p = p_{cav}$
- On the reformation border  
 $p = p_{cav} ;$  In the zone  $\Omega : p > p_{cav}$

### Oil film thickness equation

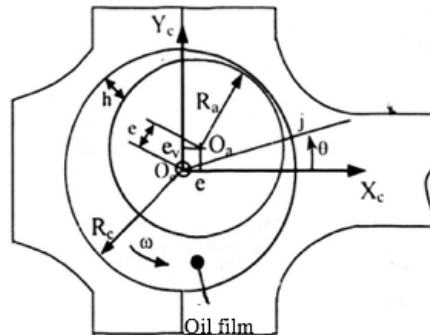


Figure 8. Scheme and cross section of a connecting-rod.

For a circular bearing (Figure.8), the thickness of the lubricant film is:

$$h = C(1 - \varepsilon_x \cos\theta - \varepsilon_y \sin\theta) \quad (5)$$

where C is the radial clearance and  $\varepsilon_x$  and  $\varepsilon_y$  are relative eccentricities.

### The equilibrium equation

The balance equation between the applied load, the resultant force of the field of hydrodynamic pressure in the film acting on the housing bearing (Figure 9) is:

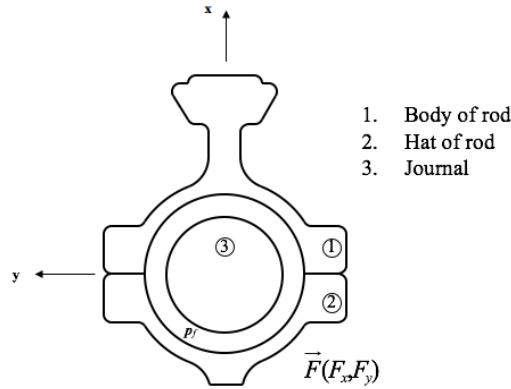


Figure 9. Scheme of the forces applied on the connecting-rod.

$$\begin{cases} F_x = \iint_{Boring} p_f \cos \theta ds \\ F_y = \iint_{Boring} p_f \sin \theta ds \end{cases} \quad (6)$$

where:  $F_x$ ,  $F_y$  are the components of the load acting on the bearing given by the load diagram,  $p_f$  is the pressure in the film.

### 3.2. Finite element formulation of the problem

The finite element method is mainly presented for the modified Reynolds equation. Consider the integral form:

$$E^* = \int_{\Omega} W^* \left( F \left( -\frac{\partial}{\partial x} \left( \frac{h^3}{6\mu} \frac{\partial D}{\partial x} \right) - \frac{\partial}{\partial z} \left( \frac{h^3}{6\mu} \frac{\partial D}{\partial z} \right) \right) + \left( U \frac{\partial h}{\partial x} + 2 \frac{\partial h}{\partial t} \right) + (1-F) \left( U \frac{\partial D}{\partial x} + 2 \frac{\partial D}{\partial t} \right) \right) d\Omega \quad (7)$$

where  $W^*$  is a sufficiently differentiable function defined on  $\Omega$

An integration by parts of certain terms, then the addition of complementary integrals defined on the transition boundaries between active and inactive zones allow the reduction on the order of derivability of the functions and to naturally create the conditions at the limits of rupture and reformation of the film [5] necessary to the treatment of the problem:

$$E(D) = \int_{\Omega} \left( F \frac{h^3}{6\mu} \left( \frac{\partial W}{\partial x} \frac{\partial D}{\partial x} + \frac{\partial W}{\partial z} \frac{\partial D}{\partial z} \right) + w \left( U \frac{\partial h}{\partial x} + 2 \frac{\partial h}{\partial t} \right) - (1-F) U D \frac{\partial W}{\partial x} \right) d\Omega - \frac{\partial}{\partial t} \int_{\Omega} 2(1-F) W D d\Omega \quad (8)$$

The functions  $W$  are chosen null on the outer boundary of the domain. The solution of the problem is obtained by looking for the inner boundaries of the film and such that  $E(D) = 0$ . The resolution of the equation  $E(D) = 0$  will make it possible to obtain the location of the active and inactive zones of the film. The domain is thus divided into isoparametric finite elements at 8 nodes. The special character of the modified Reynolds equation, when it applies to inactive zones, makes it necessary to use linear elements with four nodes for its discretization.

The selected  $N$  interpolations functions, linear or quadratic as appropriate, allow to interpolate both the geometric variables and the various parameters. The integral (8) evaluated at the node  $j$  of an element  $e$  is written:

$$\begin{aligned}
E_j(\Omega_e) = & \sum_{m=1}^{npg} \left( \frac{h^3}{6\mu} \sum_{k=1}^{nne} \left( \frac{\partial W_{mj}}{\partial x} \frac{\partial N_{mk}}{\partial x} + \frac{\partial W_{mj}}{\partial z} \frac{\partial N_{mk}}{\partial z} \right) F_k D_k \right. \\
& + W_{mj} \left( U \frac{\partial h_m}{\partial x} + \frac{h_m(t) - h_m(t-\Delta t)}{\Delta t} \right) - \sum_{k=1}^{nne} \frac{\partial W_{mj}}{\partial x} N_{mk} (1-F_k) D_k \\
& \left. - 2 \frac{1}{\Delta t} \sum_{k=1}^{nne} W_{mj} N_{mk} ((1-F_k(t)) D_k(t) - (1-F_k(t-\Delta t)) D_k(t-\Delta t)) \right) \Delta \Omega_m
\end{aligned} \tag{9}$$

where  $npg$  is number of Gauss points on the element, and  $nne$  is the number of nodes per element.  $W_{mj}$  is the weight function, and  $N_{mk}$  is the interpolation function relative to the node  $k$ .  $F_k$  presents the state of the node  $k$  and takes the value 1 if it is in an active zone and 0 in the opposite case.

The equations (9) written on each of the nodes of the  $n$  elements of the domain, which is written in the following matrix form:

$$R = [M] D + B = 0 \tag{10}$$

Let  $n$  be the total number of nodes defined on the studied domain. The matrix  $[M]$  is of rank  $n$ , a term  $M_{jk}$  is written:

$$\begin{aligned}
M_{jk} = & \sum_{n=1}^{ne} \sum_{m=1}^{npg} \left( \frac{h^3}{6\mu} \sum_{k=1}^{nne} \left( \frac{\partial N_{mj}}{\partial x} \frac{\partial N_{mk}}{\partial x} + \frac{\partial N_{mj}}{\partial z} \frac{\partial N_{mk}}{\partial z} \right) F_k + \sum_{k=1}^{nne} \frac{\partial N_{mj}}{\partial x} N_{mk} (1-F_k) \right. \\
& \left. - 2 \frac{1}{\Delta t} \sum_{k=1}^{nne} N_{mj} N_{mk} (1-F_k(t)) \right) \Delta \Omega_m
\end{aligned} \tag{11}$$

and:

$$\begin{aligned}
B_j = & \sum_{n=1}^{ne} \sum_{m=1}^{npg} \left( N_{mj} \left( U \frac{\partial h_m}{\partial x} + 2 \frac{h_m(t) - h_m(t-\Delta t)}{\Delta t} \right) \right. \\
& \left. - 2 \frac{1}{\Delta t} \sum_{k=1}^{nne} N_{mj} N_{mk} ((1-F_k(t-\Delta t)) D_k(t-\Delta t)) \right) \Delta \Omega_m
\end{aligned} \tag{12}$$

In the active zone,  $F_k = 1$ ,  $M_{jk}$  and  $B$  are written:

$$M_{jk} = \sum_{n=1}^{ne} \sum_{m=1}^{npg} \left( \frac{h^3}{6\mu} \sum_{k=1}^{nne} \left( \frac{\partial N_{mj}}{\partial x} \frac{\partial N_{mk}}{\partial x} + \frac{\partial N_{mj}}{\partial z} \frac{\partial N_{mk}}{\partial z} \right) F_k \right) \tag{13}$$

$$B_j = \sum_{n=1}^{ne} \sum_{m=1}^{npg} \left( N_{mj} \left( U \frac{\partial h_m}{\partial x} + 2 \frac{h_m(t) - h_m(t-\Delta t)}{\Delta t} \right) \right) \tag{14}$$

The equations of problem are solved by using processes of Raphson Newton. The convergence for a functional cycle is obtained if the results at the cycle end are the same as those at the beginning of the cycle.

#### 4. RESULTS

Figure 10 and Figure 11 present the connecting-rod model of photoelastic material (Figure 10) and the load diagram at rotation speed of 80 rpm and 150 rpm.

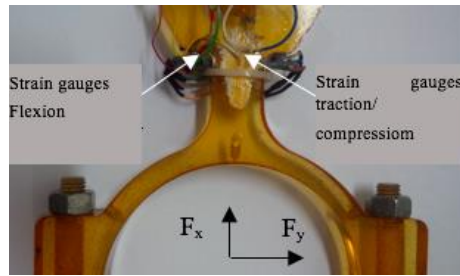


Figure 10. Connecting-rod and sensors for measuring the forces.

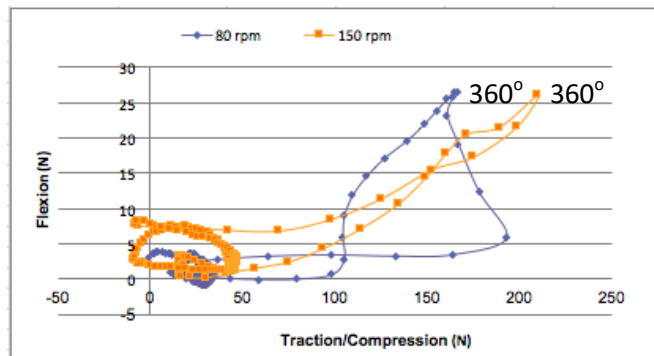


Figure 11. Load diagrams at rotation speed of 80 rpm and 150 rpm.

#### 4.1 Experimental isochrones fields



Figure 12. Isochrones field of the connecting-rod big end bearing at static situation,  $0^\circ$  of crankshaft angle.

This section presents the isochrones of connecting-rods obtained from the images taken with steps of  $30^\circ$  angle of the boring for the same crank angle. It should be noted that the continuous observation of these isochrones fields clearly shows the influence of dynamic loadings and especially the explosion.

Figure 12 represents the isochrones field in the reference position. It corresponds to a static situation at  $0^\circ$  of crankshaft angle. It is found that, despite the heat treatment carried out after the molding to eliminate the residual stresses in the connecting rod, they reappear with the time between the experiments.

When the experimental device is working, under the load apply to the connecting-rod and the pressure in the lubricant oil film change the stress in the connecting-rod during the operating cycle. Figure 13 presents the isochrones fields of the bearing at  $0^\circ$  and  $360^\circ$  crank angle for a rotation speed of 150 rpm. It shows that, the contours are darker or change the fringes, that depends on the position of the housing bearing. At the  $360^\circ$  angle of the crankshaft, a sudden change of the fringes on the rod which reflects the maximum load applied at the time of the explosion. By observing the sectors at  $30^\circ$  boring angle (Figure 14), it can count on a fringe radius 10 on the reference image and 13 fringes at the time of the explosion.

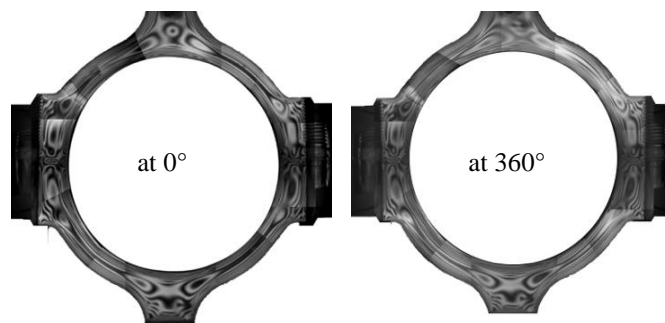


Figure 13. Bearing isochrones field at  $0^\circ$  and  $180^\circ$  of crank angle, 150 rpm.

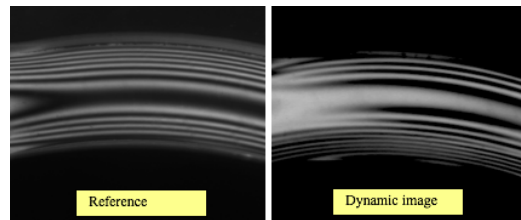


Figure 14. Isochrones field o at  $30^\circ$  of boring for  $0^\circ$   $360^\circ$  of crank angle, 150 rpm.

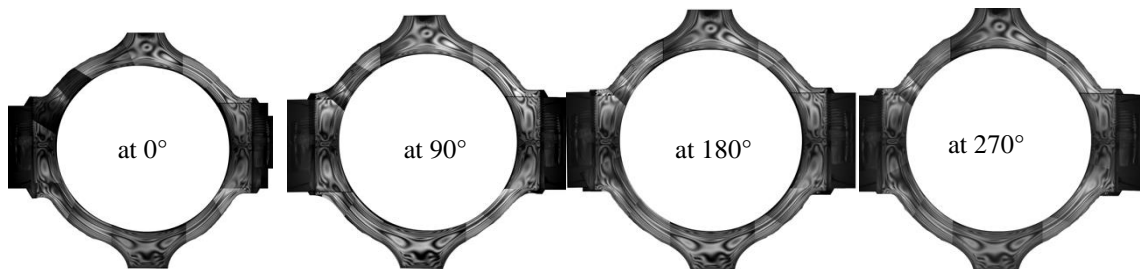


Figure 15. Isochrones fields of bearing at different crank angle with rotation speed 80 rpm.

Figure 15 represents the Isochrones fields at different crank angle with rotation speed 80 rpm. The fringes vary little, this can be explained due to the low load.

---

## 4.2 Comparison the experimental and calculated results

In transmission photoelasticity, the isochrones fringes are the result of the integration of shear throughout the thickness of the model. This is the reason why two-dimensional numerical modeling is the most appropriate for comparing isochrones fields. The photoelastic model has a shape that lends itself well to this kind of modeling because the thickness is constant. The Algor software is chosen for finite element modeling. Figure 16 presents the 2D mesh of the connecting-rod big end. The structure comprises 3357 quadrangular elements. The connecting-rod is embedding at the level of the cut of the body and to the fields of pressures.

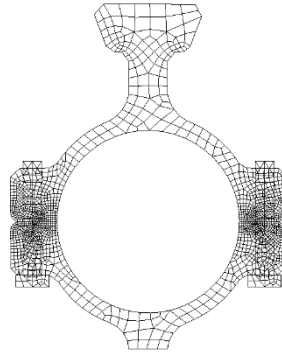


Figure 16. Mesh of the connecting-rod.

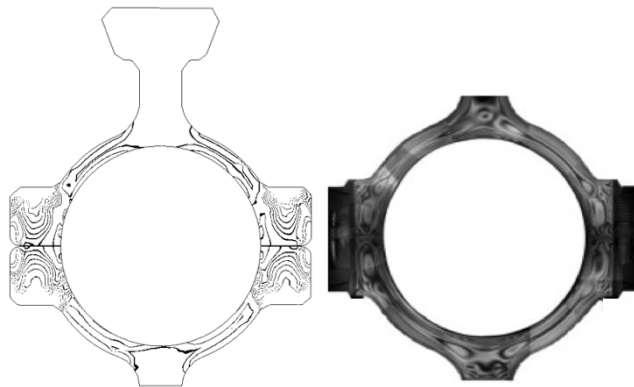


Figure 17. The reference Isochrones fields at  $0^\circ$  of crank angle, the experimental device is stopped.

The pressure fields of lubricated oil film are the results of programme by the Fortran software, for the whole operating cycle. Apply the pressure on the surfaces of the elements of the boring mesh made in the Algor software, the state of stress in the structure is obtained. This stress state can be visualized as a network of numerical fringes of isochrones or isochrones field. A comparison between the experimental isochrones field and numerical isochrones field is presents at the Figure 17. This situation corresponds to a reference state where the experimental device is stopped at  $0^\circ$  of crank angle. This qualitative comparison shows globally a fairly good correspondence between the two fields of isochrones. The fringe network is denser on the experimental field. This is mainly due to the residual stresses resulting from the different phases of obtaining the connecting rod: molding, thermal relaxation, drilling, etc.

---

Figure 18 presents the comparison of the isochrones fields of the connecting rod at the angle of the explosion -  $360^\circ$  of the crank angle for a speed of rotation of 150 rpm. For this the connecting-rod is subjected to the maximum load, isochrones fields are denser on the experimental and numerical images.

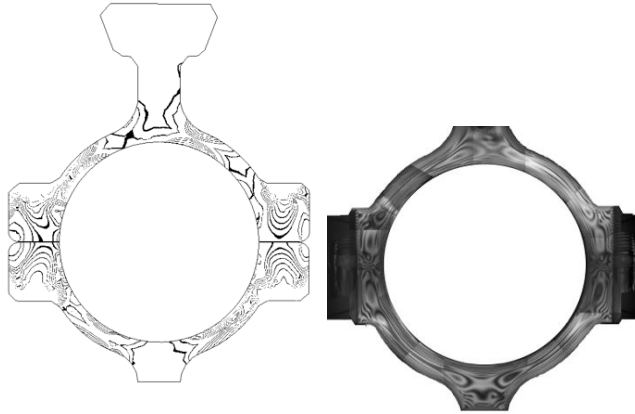


Figure 18. The Isochrones fields at  $0^\circ$  of crank angle.

## 5. CONCLUSIONS

This study investigates the stress contours of the connecting-rod model of photoelastic material in the specific experimental device for lubricating condition of the connecting-rod big end bearing. The optical methods of measurements were applied to realize this study. The method chosen to visualize the stress state in the dynamically loaded connecting rod is the transmission photoelasticity. This method allows the visualization of the isochrones fringes. Also, the numerical modeling to calculate the pressure base on solving the equations of Reynolds, of the oil film thickness, of the equilibrium of the charge. These equations are discretized by a diagram finite elements and are solved by using processes of Raphson Newton.

The stress contours of the connecting-rod are measured at different rotation speeds and at different crank angles. The experimental results show that the state of stress of the connecting-rod big is compatible with the load diagrams. Sous the dynamic load and the pressure in the lubricant oil film change the stress in the connecting-rod during the operating cycle. The contours are darker or change the number of fringes, that depends on the position of the housing bearing. At the  $360^\circ$  angle of the crankshaft, a sudden change of the fringes on the rod which reflects the maximum load applied at the time of the explosion. The sectors at  $30^\circ$  boring angle, count on a fringe radius 10 on the reference image and 13 fringes at the time of the explosion.

When the experimental device is stopped at  $0^\circ$  of crank angle, the qualitative comparison shows globally a fairly good correspondence between the experimental isochrones fields and the calculated isochrones fields. The fringe network is denser on the experimental field. This is mainly due to the residual stress resulting from the different phases of obtaining the connecting-rod: molding, thermal relaxation, drilling, etc. During the operation cycle, isochrones fields in the connecting-rod is denser on the experimental and numerical images.

**Acknowledgements.** This research is funded by the Hanoi University of Science and Technology (HUST) under project number T2018-PC-025.

---

## REFERENCES

1. Fantino B., Frêne J. - Comparison of Dynamic Behavior of Elastic Connecting-Rod Bearing in both Petrol and Diesel Engine, Transactions of the ASME Journal of Tribology **107** (1985) 87-91.
2. Oh K. P., Goenka P. K. - The Elastohydrodynamic Solution of Journal Bearings Under Dynamic Loading, Transactions of the ASME Journal of Tribology **107** (1985) 389-395.
3. Bonneau D. et Hajjam M. - Modélisation de la Rupture et de la Réformation des Films Lubrifiants dans les contacts Elastohydrodynamiques, Revue Européenne des Eléments Finis, Reef-10/2001, 2001, pp. 679-704.
4. Wang D., Keith G., Yang Q. - Lubrication Analysis of Connecting-Rod Bearing in a High-Speed Engine, Part I: Rod and Bearing Deformation, STLE Tribology Transaction **47** (2004) 280-289.
5. Thi Thanh Hai TRAN - Etude expérimentale et modélisation des interactions lubrifiée ou non entre les différents corps d'un palier de tête de bielle, Thèse de doctorat de l'Université de Poitiers, 2006.
6. Bates T.W., Fantino B. - Launay L. and Frêne J., Oil Film Thickness in an Elastic Connecting-Rod Bearing: Comparison between Theory and Experiment", STLE **33** (1990) 254-266.
7. Optasanu V. - Modélisation Expérimentale et Numérique de la Lubrification des Paliers Compliantes sous Chargement Dynamique, Thèse de Doctorat de l'Université de Poitiers, 2000.
8. Fatu A. - Modélisation numérique et expérimentale de la lubrification de palier de moteur soumis à des conditions sévères de fonctionnement, Thèse de doctorat de l'Université de Poitiers, 2005.
9. Tran Thi Thanh Hai, Nguyen Dinh Tan, Luu Trong Thuan - Influence of the radial clearance on the pressure distribution of the 5S-FE engine's connecting-rod big end bearing, Journal of Science and Technology, Technical university **132** (2019) 40-45.
10. Tran Thi Thanh Hai - A Solution for Creating the Simulating Load on Connecting-Rod in the Experimental Device for Lubricating Condition of the Connecting-Rod Big End Bearing, Journal of Science and Technology, Technical university **129** (2018) 15-20.
11. Tran Thi Thanh Hai - A solution for measuring the oil film pressure of the connecting-rod big end bearing in the experimental device, The University of Danang Journal of Science and Technology **11/2018** (1) (2018) 22-25.
12. Avril J. - Encyclopédie Vishay d'Analyse des Contraintes, Edition Vishay, Malakoff, 1975.
13. Bonneau D., Fatu A., Shouchet D. - Hydrodynamic Bearings, ISTE, London and John Wiley & Sons, New York, 2014.
14. Bonneau D., Fatu A., Shouchet D. - Internal Combustion Engine Bearings Lubrication in Hydrodynamic Bearings, ISTE, London and John Wiley & Sons, New York, 2014.